ISSN 1063-7710, Acoustical Physics, 2025, Vol. 71, No. 5, pp. 719–728. © Pleiades Publishing, Ltd., 2025.

PHYSICAL ACOUSTICS

# Compensation for Aberrations Using High-Intensity Focused Ultrasound for Destruction of Uterine Fibroids

**D. D. Chupova[a, *], P. B. Rosnitskiy[b], V. E. Sinitsyn[c], E. A. Mershina[c], O. A. Sapozhnikov[a], and V. A. Khokhlova[a]**

[a] *Faculty of Physics, Moscow State University, Moscow, 119991 Russia*

[b] *Division of Gastroenterology, Department of Medicine, University of Washington School of Medicine, Seattle, WA, 98195 USA*

[c] *University Clinic of Medical Research and Educational Institute, Moscow State University, Moscow, 119192 Russia*

**e-mail: daria.chupova@yandex.ru*

Received September 21, 2024; revised May 7, 2025; accepted June 24, 2025

**Abstract**—In a numerical experiment, we analyzed the distortion of an ultrasound beam when focusing through the abdominal wall into the area of uterine fibroids and assessed the possibility of compensation for aberrations caused by inhomogeneities of human body tissues. A three-dimensional acoustic model of the female pelvic organs was constructed based on anonymized CT data. The field was calculated by combining the analytical method for calculating the Rayleigh integral and the pseudospectral method for solving the wave equation in an inhomogeneous medium (*k*-Wave software package). The diffraction algorithm for aberration compensation was based on modeling the propagation of a spherical wave from the focal point to the surface of an ultrasound phased array and optimizing the selection of phases on its elements using the least squares method. A model of a 256-element compact array with an operating frequency of $f = 1.2$ MHz and an aperture number of $F\# = 0.75$ was used. Significant field distortions and the occurrence of side maxima comparable in amplitude to the main one are demonstrated in the absence of aberration compensation. Compensation for aberrations made it possible to ensure precise focusing in the target area and increase the pressure amplitude at the focus by 3.2 times.

**Keywords:** medical acoustics, high-intensity focused ultrasound, multielement phased array, computed tomography, uterine fibroids, numerical modeling

**DOI:** 10.1134/S1063771024602772

## INTRODUCTION

Uterine fibroids are one of the most common pathologies of the female reproductive system. It is a hormonally dependent benign formation of smooth muscle and connective tissue, occurring in more than 70% of women by the end of the reproductive period [1, 2]. The disease is often asymptomatic; however in approximately 30% of cases, it has pronounced clinical symptoms, including the development of anemia, pain, pressure in the pelvic area, infertility, and dysfunction of adjacent organs (bladder and rectum) [2, 3]. The main approaches to treating symptomatic uterine fibroids at present are hormone therapy, hysterectomy (surgical removal of the uterus), myomectomy (minimally invasive removal of fibroids if small in size and in an easily accessible location), uterine artery embolization, and minimally invasive thermal radioablation under ultrasound control [3]. Like any surgical intervention, invasive and minimally invasive procedures carry the risk of complications such as infection and bleeding, loss of reproductive function, and a long recovery period. Hormonal therapy and myomectomy are characterized by a high rate of disease recurrence [4, 5]. Thus, the development of completely non-invasive organ-preserving treatment methods is of particular interest in modern surgery.

One such method for treating fibroids is HIFU controlled by MRI thermometry [6–8]. During the procedure, an ultrasound beam is focused through the abdominal wall into a specific area of the tumor using a multielement transducer array, causing local tissue heating and subsequent necrosis. To destroy clinically significant tumor volumes, the transducer focus is sequentially moved along a discrete trajectory, and irradiation is repeated until the entire specified volume is destroyed [8]. The use of transducers in the form of multielement phased arrays allows for moving the focus both mechanically and electronically by introducing appropriate phase delays on each of the elements. In this case, the aperiodic arrangement of elements makes it possible to avoid the occurrence of side diffraction lobes [9, 10]. This procedure is completely non-invasive, allows for reduction of disease symptoms, ensures a quick recovery period, and reduces the risk of serious complications compared to invasive methods [11].

Although the HIFU method has already been successfully used in clinical practice, it has a number of limitations. Since the primary mechanism of tissue destruction is thermal ablation, the method is most effective for tissues with strong absorption of ultrasound energy and a relatively low level of perfusion. In the case of uterine fibroids, these are ordinary, dark on T2-weighted MRI, fibroids [8]. At the same time, the effectiveness of thermal ablation for hypercellular (white on T2-weighted MRI) fibroids, in the nodules of which intensive growth of blood vessels occurs, is very low due to the weak absorption of ultrasound in such fibroid tissues; therefore, HIFU therapy is not used for them [12]. Significant limitations to the applicability of HIFU also include heterogeneity of the acoustic parameters of muscular and fatty tissue of the abdominal wall along the beam path, associated with differences in sound speed, limited size of the acoustic window, as well as tumor heterogeneity and the presence of calcifications. The presence of inhomogeneities leads to strong distortion (aberration) of the field and unpredictable redistribution of thermal sources: displacement and blurring of the planned focus, formation of additional zones with increased field amplitude [8, 12]. In addition, difficult-to-control heat diffusion processes leading to unwanted overheating of adjacent tissues, as well as the high cost of operation owing to MRI scanning and the limitations associated with its implementation, also reduce the availability of the procedure to patients [8, 13]. Thus, an important challenge is to develop new non-invasive methods to treat myomas using focused ultrasound with the potential to diminish the limitations associated with heat diffusion and perfusion, large differences in tissue absorption coefficients, and the use of cost-intensive MRI guidance. A separate important task is the development of methods for correcting aberrations.

One of the recently proposed methods that could potentially overcome the existing limitations of thermal HIFU is the boiling histotripsy (BH) method for mechanical tumor destruction [14]. This method uses a sequence of short, high-amplitude pulses lasting several milliseconds. Near the focus, due to the nonlinearity of the propagation medium, shock fronts form in the acoustic pressure waveform. Efficient absorption of ultrasound wave energy at the shock fronts leads to rapid heating and local boiling of tissue at the focus during each pulse. The interaction of shock fronts with the resulting vapor-gas cavities leads to the mechanical destruction of tissue into subcellular fragments: its liquification occurs. The effects of heat diffusion and perfusion in BH are not significant, since the main mechanism of tissue destruction is mechanical, and the primary shock wave heating of tissue is localized within the focal region of the beam and occurs very quickly [14, 15]. The vapor-gas cavities formed in the tissue during BH irradiation are hyperechoic for diagnostic ultrasound, and after irradiation, the liquefied tissue contains almost no scatterers and therefore becomes hypoechoic. The high contrast of the exposure region during and after irradiation makes it possible to monitor the BH procedure using diagnostic ultrasound (US) sensors, which are usually located in the center of the BH transducer, as well as to consider diagnostic ultrasound a potential replacement for the expensive MRI method [16]. The fundamental possibility of using BH for the destruction of human uterine leiomyoma ex vivo using ultrasound guidance has recently been demonstrated experimentally [17].

An important condition for the successful implementation of BH is to ensure coherent accumulation of nonlinear effects, which is necessary to generate high-amplitude shock fronts at the focus. Considering the high requirements on the acoustic power of the transducer and limited acoustic window associated with the presence of pelvic bones in the ultrasound path, the surface of the ultrasound transducer should be filled as densely as possible with elements, while being randomly located to ensure an acceptable range of electronic focus steering without the formation of side lobes [18]. In recent studies by the Laboratory for Industrial and Medical Ultrasound of Lomonosov Moscow State University, a computer model was developed, and a 256-element transducer was manufactured having absolutely dense mosaic filling of the surface with elements—polygons with the same area, located randomly (Fig. 1) [18, 19]. The operating frequency, geometry, and dimensions of the array ($f$ = 1.2 MHz, focal length $F$ = 150 mm, diameter $D$ = 200 mm, and diameter of the central aperture $d$ = 40 mm) are close to the parameters of the Sonalleve MR-HIFU clinical system (Profound Medical, Canada) [20]; therefore, the manufactured transducer can be considered as a prototype of a clinical BH system with ultrasound monitoring for the mechanical destruction of deep-seated uterine fibroids.

The aim of this study was to investigate in a numerical experiment the possibility of using this transducer to solve the problem of compensating for aberrations and ensuring precise focusing of the ultrasound beam in the area of uterine fibroids. The problem of linear beam focusing was considered. However, as shown earlier, compensation of aberrations in a linear beam also allows for the efficient implementation of nonlinear focusing regimes [21]. The modeling was performed using a realistic three-dimensional acoustic model of the pelvic organs, constructed based on anonymized computed tomography (CT) data. The influence of the heterogeneity of the abdominal wall and also the partial overlap of the beam by the pelvic bones on the distortion of the field in focus, the possibility of compensating for aberrations and the potential feasibility of the procedure were analyzed.

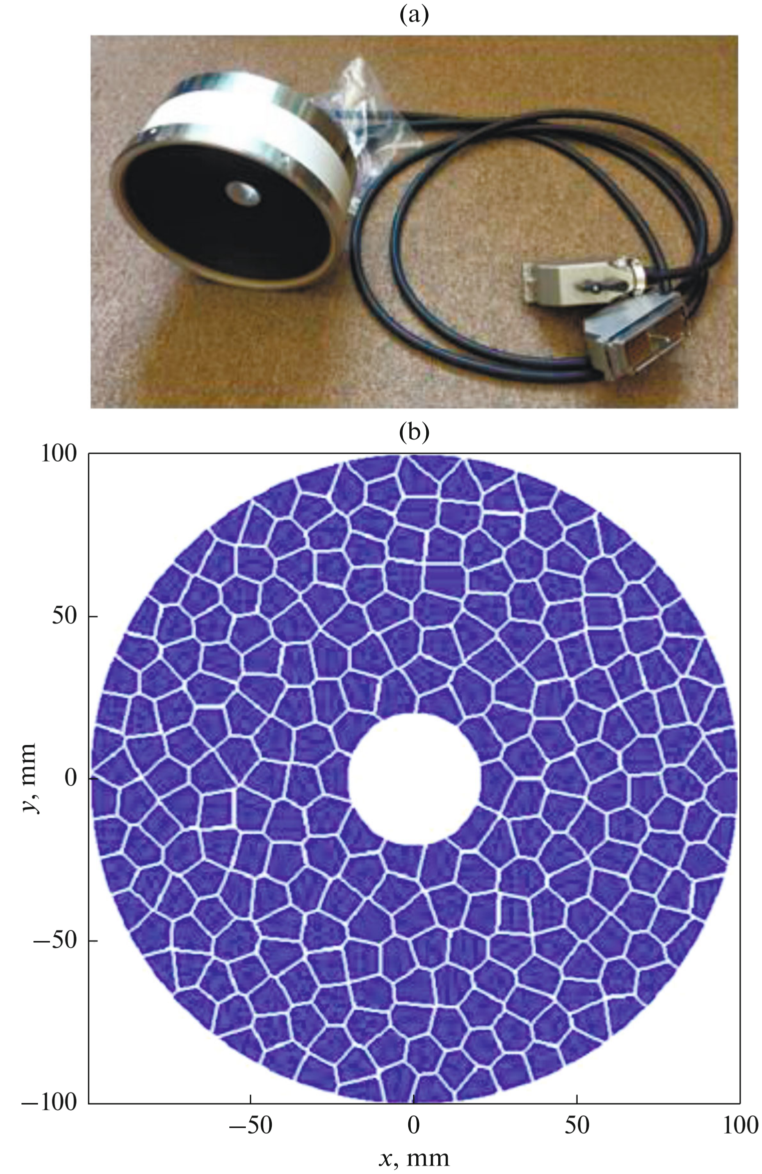


**Fig. 1.** (a) Photograph of ultrasound transducer in form of 256-element mosaic array. (b) Schematic diagram of arrangement of elements on transducer surface.

## THEORETICAL MODEL

### *Construction of an Acoustic Model Based on Computed Tomography Data*

To construct a three-dimensional acoustic model of the pelvic organs, anonymized computed tomography (CT) data from an 85-year-old female patient were used (archive material, IRB exempt). The data were provided by the University Clinic of the Medical Scientific and Educational Institute, Lomonosov Moscow State University, and consisted of 417 axial sections with a resolution of $0.68 \times 0.68 \times 1$ mm (Fig. 2). The data were obtained during a routine examination of the patient using a 128-row SOMATOM Drive CT scanner (Siemens, Erlangen, Germany).

CT is based on recording the attenuation of an X-ray beam as it passes through biological tissues. The quantitative characteristic of the degree of weakening is the Hounsfield scale. It is known that Hounsfield units (HU) correlate with the density of biological tissue, and the density correlates with the velocity of longitudinal sound waves [22]. Thus, information about the distribution of density and sound velocity in each voxel of the image can be obtained from CT data. Due to the lack of correlation between HU and the absorption coefficient, a different method was used to create the acoustic absorption model. First, the 3D CT data were segmented into different tissue and organ types using the open-source software 3D Slicer (slicer.org) [23].

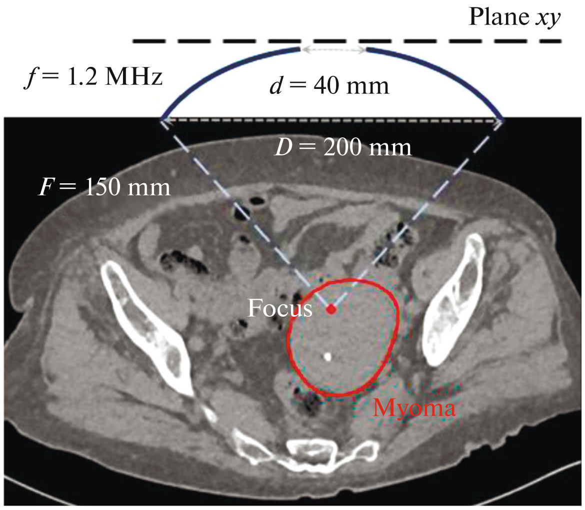


**Fig. 2.** Axial CT scan of pelvic organs; area of uterine fibroid is marked with a red outline. Dashed lines show geometry of a focused ultrasound beam generated by transducer with operating frequency of $f = 1.2$ MHz, focal length $F = 150$ mm, diameter $D = 200$ mm, and aperture diameter $d = 40$ mm. Plane *xy* passes through apex of transducer (point on spherical radiating surface through which transducer axis passes) perpendicular to specified axis.

Then, each segment was assigned values taken from the reference literature [24, 25].

For further calculations, CT and segmentation data were interpolated onto a uniform computational grid with a step of $\Delta x = \Delta y = \Delta z = 0.4$ mm. The grid step was chosen in such a way as to satisfy the condition $\lambda_0/3$, which ensures sufficient accuracy of further calculations in the *k*-Wave software package (*k*-wave.org) [26], where $\lambda_0 = c_0/f_0$ is the ultrasound wavelength, $f_0 = 1.2$ MHz is the transducer operating frequency, and $c_0 = 1500$ m/s is the characteristic sound speed in soft tissues. After interpolation onto the computational grid based on the CT data, two three-dimensional matrices were created: a density matrix and a sound velocity matrix, calculated from HU. Based on the segmentation results, a three-dimensional absorption coefficient matrix was created.

Taking into account that in the case under consideration the beam path was through a gas-filled intestine, changes were made to the model to simulate a realistic surgical process. Since gas cavities almost completely reflect and scatter ultrasound, in clinical conditions the intestine is filled with a matching fluid, and if there are residual gas cavities, they are displaced from the zone of influence by changing the patient's position [27]. To model this procedure, voxels with sound speed values less than 1412 m/s, corresponding to the minimum sound speed in soft tissues along the beam path, were identified in the CT data. Then, such voxels were assigned acoustic parameters of water [28]. The resulting three matrices—density, sound velocity, and absorption coefficient—had dimensions of 730 × 730 × 412 points, which corresponded to a spatial modeling area of 291.6 × 291.6 × 164.4 mm.

### *Field Calculation and Aberration Compensation Methods*

As mentioned above, the transducer considered in the study was a 256-element array with an operating frequency of $f_0 = 1.2$ MHz, diameter $D = 200$ mm, focal length $F = 150$ mm, and absolutely dense filling of the surface with polygonal elements of equal area [19]. In the center of the transducer was an aperture with a diameter of $d = 40$ mm for placement of the ultrasound diagnostic probe [16, 19–21]. Figure 2 shows the geometry of the numerical experiment.

Field calculations and aberration compensation were performed using the *k*-Wave (http://www.k-wave.org) [26, 29]. This complex implements a numerical pseudospectral method for solving a system of linear acoustics equations:

$$\begin{cases} \dfrac{\partial \mathbf{u}}{\partial t} = -\dfrac{1}{\rho_0(\mathbf{r})}\nabla p, \\ \dfrac{\partial \rho}{\partial t} = -\rho_0(\mathbf{r})\nabla \mathbf{u} - \mathbf{u}\nabla\rho_0(\mathbf{r}) + M(\mathbf{r},t), \\ p = c_0^2\left(\rho + \mathbf{d}\nabla\rho_0(\mathbf{r}) + 2\alpha_0(\mathbf{r})c_0(\mathbf{r})\dfrac{\partial\rho}{\partial t}\right), \end{cases} \tag{1}$$

where $\boldsymbol{u}$ is the vibrational velocity of particles of the medium, $\rho_0(\mathbf{r})$ is the density of the medium depending on the radius vector $\mathbf{r}$, $p$ is the acoustic pressure, $\rho$ is the acoustic density perturbation, $\mathbf{d}$ is the displacement of particles of the medium (i.e.m $\mathbf{u} = \partial\mathbf{d}/\partial t$), $c_0(\mathbf{r})$ is the sound speed, $\alpha_0(\mathbf{r})$ is the parameter for calculating the absorption coefficient $\alpha = 4\pi^2\alpha_0 f_0^2$, and $M(\mathbf{r}, t)$ represents "mass sources" describing the ultrasound source.

The three-dimensional calculation domain was given in Cartesian coordinates. The step of the spatial computational grid was the same in all directions: $\Delta x = \Delta y = \Delta z = 0.4$ mm; its size was 730 × 730 × 412 points. The computational grid was surrounded on each side by a perfect matching layer (PML) occupying ten points in each direction. The step of the time grid was chosen according to the Courant–Friedrichs–Lewy criterion and satisfied the condition $\mathrm{CFL} = 0.3$, where $\mathrm{CFL} \equiv c_{max}\Delta t/\Delta x$, $c_{max}$ is the maximum sound speed in the model, which is a criterion for the stability of calculations for the numerical scheme used [29].

At the first stage of modeling, the field propagated from the spherical surface of the array to the *xy* plane, tangent to the transducer at its apex and located in the water at $z = 0$ (Fig. 2). This step was necessary to avoid the error associated with inaccurate specification of the spherical surface at the nodes of the equidistant mesh in Cartesian coordinates. The phases on the array elements were set to zero, and the normal component of the vibrational velocity on the $xy$ plane was calculated using the Rayleigh integral [28, 30]. The normal component of the vibrational velocity $u_n$ is related to the sources of mass $M(\mathbf{r}, t)$ as follows [28]:

$$M(x,y,t) = \frac{2\rho_{\text{water}} u_n(x,y,t)}{\Delta x}, \quad (2)$$

where $\rho_{\text{water}}$ is the density of water, $\Delta x$ is the step of the computational grid. In the software package $k$-Wave, the wave source is given by the pressure matrix source.p and can be expressed as $0.5c_{\text{water}}\Delta x M$ [26]. After setting the boundary condition on the $xy$ plane tangent to the transducer, ultrasound propagation through a matching layer of water and further in the inhomogeneous medium of the human body was modeled without compensation for aberrations. The results were used to analyze the influence of aberration effects on focusing distortion.

Aberration compensation then was carried out in three stages. First, using the field calculation data in the absence of aberration compensation, the position of the field maximum inside the myoma was found, which is always slightly different from the center of curvature of the transducer. It has been previously shown that, compared to focusing at the geometric center of the transducer, focusing at the maximum point after aberration compensation allows for a larger pressure amplitude to be obtained at the target point [28]. Therefore, after the coordinates of the field maximum were found, a point harmonic source $M \sim \sin(2\pi f_0 t)$ was placed at this point, then propagation of a spherical wave to the $xy$ plane was modeled using the $k$-Wave (Fig. 2). At the third stage, the phases on the array elements were selected to best reproduce the obtained distribution of the complex pressure amplitude on the $xy$ plane. To speed up the calculations, a combination of the analytical method for solving the Rayleigh integral and the least squares method was used [10, 28]. First, assuming wave propagation in water, the field from the $xy$ plane was transferred using the Rayleigh integral to a parallel $x'y'$ plane located at a distance $z = F/2$ in the far field of each of the array elements, and was represented as a linear combination of analytical solutions for each of the elements with variable amplitude and phase: $\hat{p}_i = \sum_{j=1}^{N} C_{ij}\hat{u}_j$, where $\hat{p}_i$ are the complex pressure amplitudes at the nodes of the calculation plane $z = F/2$; the coefficients $C_{ij}$ are known and depend on the relative position of the transducer element and the node on the plane; $\hat{u}_j$ are the complex amplitudes of the vibrational velocity on the transducer elements; $i = 1,\ldots,N_{x,y}^2$, where $N_{x,y} = 730$ is the number of mesh nodes, the same along the $Ox$ and $Oy$ axes; $j = 1,\ldots,N$, where $N = 256$ is the number of transducer elements. Equating the obtained complex pressure amplitudes at each of the grid nodes on the plane $x'y'$, a system of equations for the amplitudes of the vibrational velocity $\hat{u}_j$ was obtained on the array elements. Since the number of grid nodes on the $x'y'$ plane (system equations) is significantly greater than the number of array elements (unknown quantities), then the system is overdetermined. The most accurate solution was sought using the least squares method and it is described in detail in [28, 31]. Complex amplitudes of the vibrational velocity were obtained for each transducer element, while the obtained velocity phases were inverted and the amplitude on the elements was set equal for all elements. Next, the field calculation was carried out taking into account the obtained aberration compensation.

## RESULTS

### *Verification of the Accuracy of Numerical Solution to the Problem Based of Focusing in Water*

To check the correctness of the choice of spatial and temporal steps of numerical modeling, the results of field calculations obtained using $k$-Wave and the Rayleigh integral were compared. The modeling was done for the case of focusing in water, and all array elements radiated in phase. Figure 3 shows the distribution of the pressure amplitude normalized to the characteristic pressure amplitude on the surface of the array $p_A/p_0$, $p_0 = v_0 c_0 \rho_0$, where $v_0$ is the amplitude of the vibrational velocity on a transducer element, along the $Oz$ axis, and in the transverse direction along the $Ox$ axis in the focal plane of the transducer. Clearly, the results obtained in $k$-Wave (points on graph) agree well with the results of calculating the field using the Rayleigh integral (solid lines). Differences in the values of the normalized pressure amplitude $p_A/p_0$, including the maximum field $p_{\max}/p_0 = 170.9$ ($k$-Wave) and $p_{\max}/p_0 = 171.0$ (Rayleigh integral), are less than 1%.

### *Acoustic Model of Abdominal and Pelvic Tissues*

The acoustic model of the abdominal and pelvic tissues, based on segmentation of three-dimensional CT data into different tissue types, is shown in Fig. 4. The position of the transducer relative to the patient's body is also shown. For convenience, the figure shows only segments of bone and digestive gases in the intestine; the geometric center of the transducer is marked in red. Clearly, the irradiation cone (marked in dark blue) includes a bone segment the acoustic properties of which differ most significantly from those of the surrounding soft tissue. The largest bone area in the irradiation cone is 13 cm$^2$ at a distance of 55 cm from the focus or 17% of the cross-sectional area of the cone at this distance.

Figure 5 shows two-dimensional sections of a three-dimensional acoustic model based on a section in the $zy$ plane, where the $Oz$ axis is the transducer

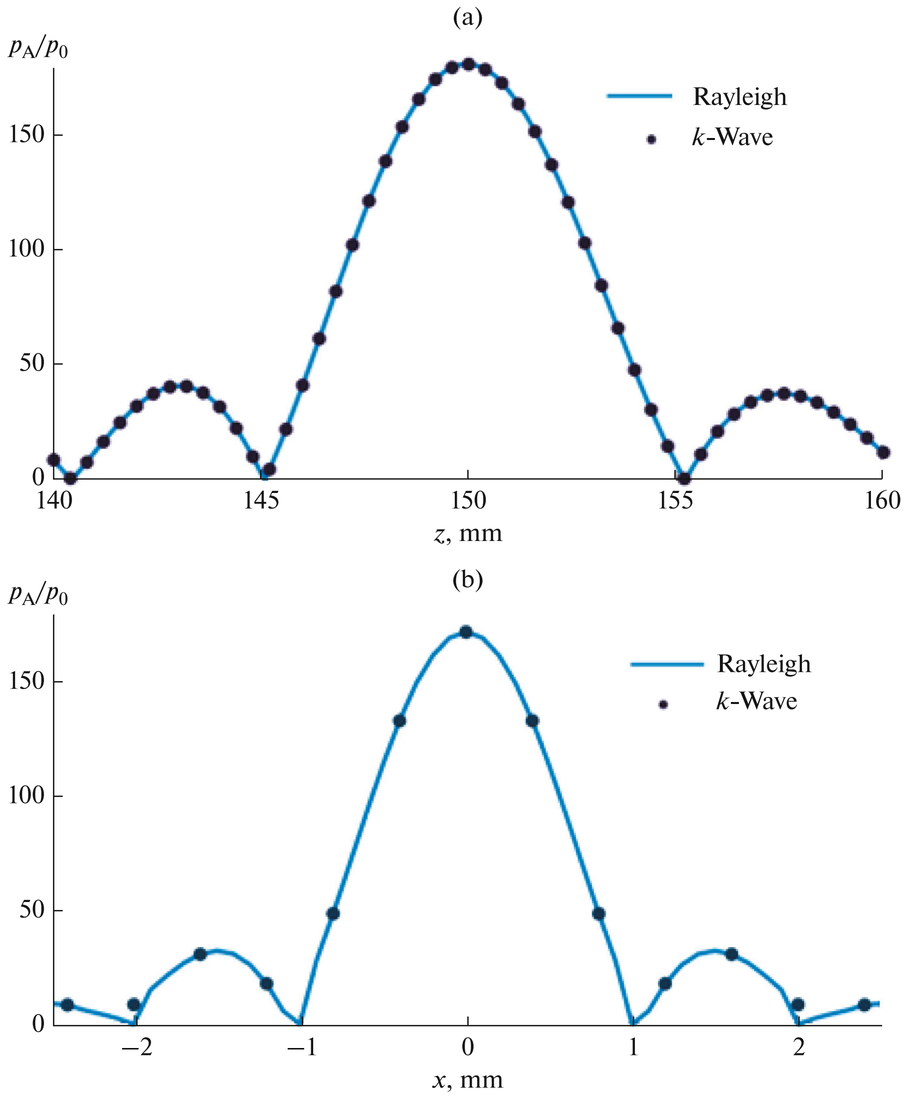


**Fig. 3.** Numerically calculated (in $k$-Wave) distribution of normalized pressure amplitude $p_A/p_0$ for focusing in water (dots) compared to analytical solutions (solid curves): (a) along transducer axis $Oz$, (b) in transverse direction $Ox$ in focal plane.

axis. As a result of segmentation, the following segments were identified: *1*, water (external medium); *2*, skin; *3*, fat; *4*, other tissues (including myoma); *5*, bone; *6*, gas (Fig. 5a). The density and sound speed distributions in the same plane are shown in Figs. 5b and 5c, respectively. Moreover, as mentioned above, areas with the sound speed below 1412 m/s were filled with water. Thus, in the calculation matrix, the entire "gas" segment and areas of other segments with low sound speed had the acoustic parameters of water, $\rho_0 = 1000$ kg/m$^3$ and $c_0 = 1500$ m/s. The absorption coefficient for water was assumed to be zero, $\alpha = 0$ dB/cm. For soft tissues (segment 4, "other tissues"), the average sound speed was $c_{\rm o.tiss} = 1550$ m/s; for fat, $c_{\rm fat} = 1450$ m/s; for skin, $c_{\rm skin} = 1500$ m/s; and for bone, $c_{\rm bone} = 1800$ m/s [22, 25]. The absorption coefficients were: $\alpha_{\rm o.tiss} = 0.7522$ dB/cm for tissue, $\alpha_{\rm fat} = 0.4614$ dB/cm for fat, $\alpha_{\rm skin} = 2.205$ dB/cm for skin, and $\alpha_{\rm bone} = 5.081$ dB/cm for bone [24, 25].

### *Focusing of the Ultrasound Beam into Uterine Fibroid Tissue*

When modeling the focusing of an ultrasound beam in uterine fibroid tissue without compensation for aberrations, pressure amplitude distributions $p_A/p_0$, normalized to the pressure amplitude on the transducer elements, were obtained in two axial planes of the transducer $zy$ and $zx$ and in the transverse plane $xy$, passing through the maximum of the field generated by the transducer. Figure 6 shows the $p_A/p_0$ distributions in the three planes $zy$, $zx$, $xy$. It can be seen that the field is highly distorted, the focal region is blurred, there is no single distinct focus, and many additional field pressure maxima arise. In this case, the maxi-

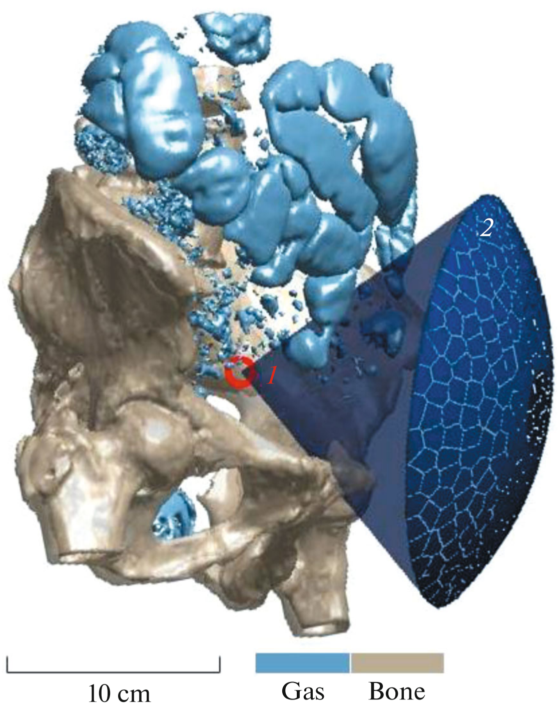


**Fig. 4.** Geometry of irradiation of uterine fibroids in numerical experiment. Irradiation cone is highlighted in dark blue. Legend: (*1*) position of geometric focus of ultrasound transducer in form of 256-element array; (*2*) spherical surface of transducer with mosaic distribution of elements.

mum pressure amplitude achievable with such irradiation is $p_{max}/p_0 = 12.1$, which is 7% of the case of focusing in water without losses. At the same time, there are numerous side maxima aside from the main one, which are comparable with it in amplitude. Thus, a maximum is observed that is almost equal to the main one, ($p_A/p_0 = 12.1$), which is located at a distance of 1.2 cm from it. For clinical practice, this means that if regimes sufficient for tissue destruction are achieved in the area of the main maximum of the field, tissue will also be destroyed outside the target area. Such irradiation may affect organs outside the target treatment area and would be unsafe for patients. Therefore, to implement an operation using HIFU, it is necessary to take into account the presence of aberrations introduced by acoustic inhomogeneities of tissues and compensate for them.

Aberration compensation was performed for the point of the main maximum of the field obtained in the simulations without aberration compensation. The main maximum was shifted with respect to the geometric center of the transducer by 1.2 mm along the *Oy* axis and by –4 mm along the *Oz* axis. There was no displacement along the *Ox* axis. Figure 7 shows the result of the $p_A/p_0$ distribution in the three planes *zy*, *zx*, *xy*. Clearly, after aberration compensation, a single field maximum is formed, with the gain being equal to $p_{max}/p_0 = 39.0$, which is 23% of the focusing case in water. Thus, the previously proposed aberration compensation algorithm allows for precise focusing and

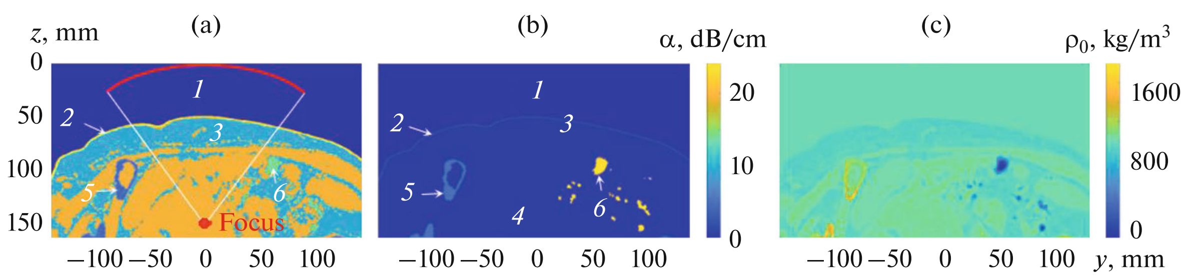


**Fig. 5.** (a) Result of segmentation of CT data by tissue types using example of slice in *zy* plane: (*1*) water (dark blue); (*2*) skin (yellow); (*3*) fat (light blue); (*4*) other tissues (orange); (*5*) bone (blue); (*6*) gas (green). (b) Distribution of absorption coefficient α corresponding to segmentation. Numerals indicate different media. (c) Density distribution $\rho_0$, calculated from HU.

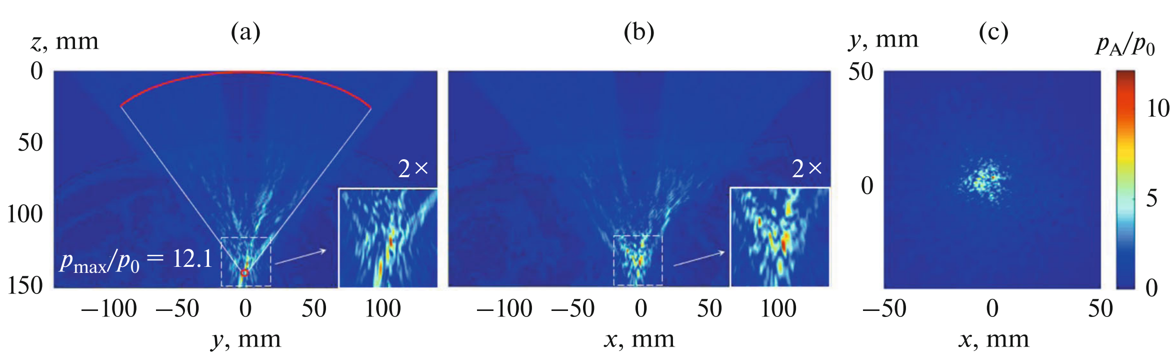


**Fig. 6.** Distributions of normalized pressure amplitude $p_A/p_0$ for irradiatiation without compensation for aberrations in three planes: (a) *zy* ($x = 0$ mm); (b) *zx* ($y = 1.2$ mm); (c) *xy* ($z = 146$ mm); symbol o marks geometric focus of transducer.

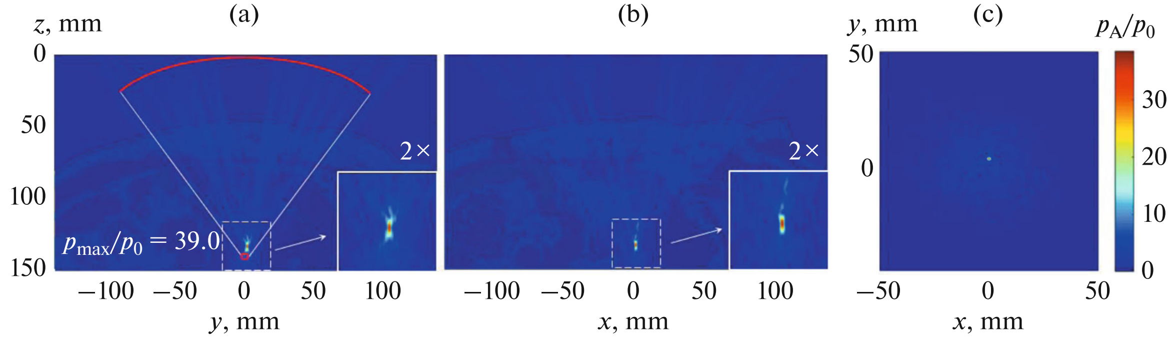


**Fig. 7.** Distributions of normalized pressure amplitude $p_A/p_0$ for irradiation with compensation for aberrations in three planes: (a) $zy$ ($x = 0$ mm); (b) $zx$ ($y = 1.2$ mm); (c) $xy$ ($z = 146$ mm); symbol o marks geometric focus of transducer.

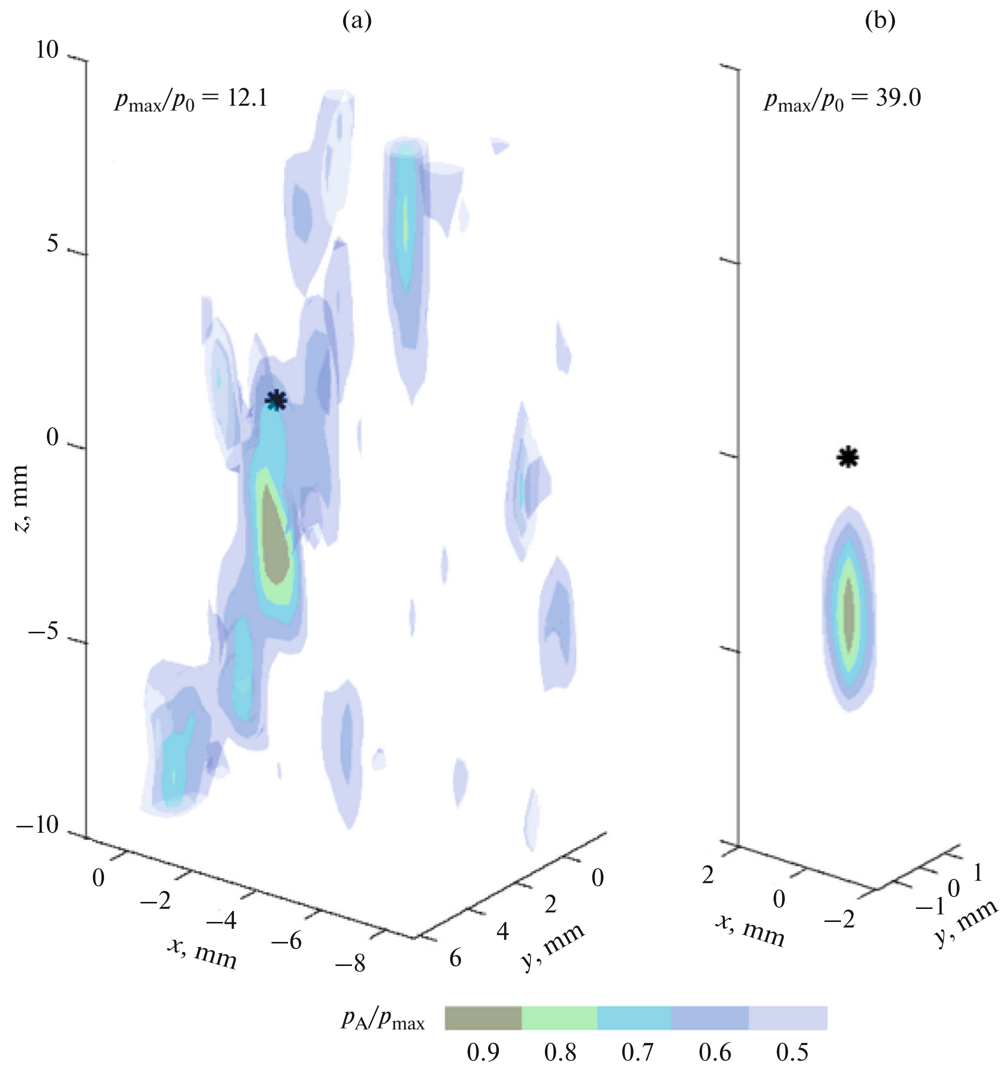


**Fig. 8.** Three-dimensional distributions of pressure amplitude $p_A/p_{max}$, normalized to maximum pressure, in cases (a) without compensation for aberrations and (b) after compensation for aberrations. Geometric focus of transducer is marked with *.

increases the maximum pressure amplitude in this example by 3.2 times compared to the case without compensation.

Figure 8 shows a comparison of three-dimensional distributions of the pressure amplitude $p_A/p_{max}$, normalized to the maximum value of the field pressure in the focal region, for cases of simulations without and after compensation of aberrations. It can be seen that compensation of aberrations allows for obtaining a localized focal region in the target area (Fig. 8b), the width of which at half-height does not exceed 1.5 mm, and the length is about 6.0 mm, which corresponds to the case of focusing in water (Fig. 3).

## CONCLUSIONS

The paper presents a numerical experiment on focusing an ultrasound beam into the area of a uterine fibroid using a new class of multielement transducer in the form of a randomized mosaic array with an absolutely dense filling of elements. Using anonymized CT data from a patient with myoma as an example, an acoustic model was constructed, the influence of inhomogeneous layers of the abdominal wall on the distortion of the focal region of the beam was analyzed, and the focusing quality was assessed after aberration compensation. The accuracy of numerical calculations and setting boundary conditions in the *k*-Wave software package was verified using calibration calculations in water and comparison with analytical solutions.

It was shown that the presence of layers of fatty and muscle tissue inhomogeneous in thickness and structure of tissue layers along the beam path leads to strong distortions of the focal region of the beam and the appearance of additional field maxima comparable in magnitude to the main one. The proposed aberration compensation algorithm made it possible to reconstruct the focal region, corresponding in length and width to focusing in water, and to increase the pressure amplitude at the target point by 3.2 times. The development of the proposed approach has the potential to increase the number of cases that can be treated using thermal HIFU and appears critically important for the clinical use of new nonlinear irradiation protocols in BH modes. In future studies of the clinical use of BH to treat fibroids, it is planned to collect statistics in a numerical experiment based on CT data from various patients, modeling the creation of volumetric destruction using electronic and mechanical steering of the focus, as well as further implementation of irradiation of uterine fibroid samples ex vivo with the achievement of BH modes.

## FUNDING

The study was supported by the Russian Science Foundation, grant no. 20-12-00145, in development of an aberration correction method, project no. 23-SCH06-02 of the Moscow State University Program of Development and the scholarship no. 22-2-10-6-1 of the Basis Foundation for postgraduate students in the processing of CT data.

## CONFLICT OF INTEREST

The authors of this work declare that they have no conflicts of interest.

## REFERENCES

1. N. V. Aganezova, S. S. Aganezov, and M. M. Shilo, Probl. Reprod. **28** (4), 97–105 (2022).
2. E. A. Stewart, C. L. Cookson, R. A. Gandolfo, and R. Schulze-Rath, Int. J. Obstet. Gynaecol. **124**, 1501 (2017).
3. J. Donnez and M. M. Dolmans, Hum. Reprod. Update **22**, 665 (2016).
4. K. J. Kramer, S. Ottum, D. Gonullu, et al., PLoS One **16**, e0261085 (2021).
5. W. Yan, S. Yuan, D. Zhou, et al., BMJ Open **14**, e081736 (2024).
6. D. M. Matlac, T. Tonguc, N. Mutschler et al., J. Clin. Med. **12**, 5926 (2023).
7. L. Liao, Y. H. Xu, J. Bai, P. Zhan, J. Zhou, M. X. Li, and Y. Zhang, Clin. Radiol. **78** (1), 61 (2023).
8. T. V. Sycheva, V. E. Sinitsyn, and E. A. Mershina, Diagn. Intervent. Radiol. **3** (2), 77–87 (2009).
9. L. R. Gavrilov and J. W. Hand, IEEE Trans. Ultrason. Ferroelectr. Freq. Control **47**, 125 (2000).
10. S. A. Ilyin, P. V. Yuldashev, V. A. Khokhlova, L. R. Gavrilov, P. B. Rosnitskiy, and O. A. Sapozhnikov, Acoust. Phys. **61**, 52 (2015).
11. Y. Ji, K. Hu, Y. Zhang, L. Gu, J. Zhu, L. Zhu, Y. Zhu, and H. Zhao, Arch. Gynecol. Obstet. **296**, 1181 (2017).
12. L. E. Rueff and S. S. Raman, Semin. Intervent. Radiol. **30**, 347 (2013).
13. C. Y. Kong, L. Meng, Z. B. Omer, J. S. Swan, S. Srouji, G. S. Gazelle, and F. M. Fennessy, Am. J. Roentgenol. **203**, 361 (2014).
14. T. D. Khokhlova, M. S. Canney, V. A. Khokhlova, O. A. Sapozhnikov, L. A. Crum, and M. R. Bailey, J. Acoust. Soc. Am. **130**, 3498 (2011).
15. M. S. Canney, V. A. Khokhlova, O. V. Bessonova, et al., Ultrasound Med. Biol. **36**, 250 (2010).
16. C. R. Bawiec, et al., IEEE Trans. Ultrason. Ferroelectr. Freq. Control **68** (5), 1496 (2021).
17. E. Ponomarchuk, S. Tsysar, A. Kvashennikova, et al., Ultrasound Med. Biol. **50**, 1255 (2024).
18. P. B. Rosnitskiy, B. A. Vysokanov, L. R. Gavrilov, O. A. Sapozhnikov, and V. A. Khokhlova, IEEE Trans. Ultrason. Ferroelectr. Freq. Control **65**, 630 (2018).
19. S. A. Tsysar, P. B. Rosnitskiy, S. A. Asfandiyarov, et al., Acoust. Phys. **70**, 82 (2024).
20. M. M. Karzova, W. Kreider, A. Partanen, T. D. Khokhlova, O. A. Sapozhnikov, P. V. Yuldashev, and V. A. Khokhlova, IEEE Trans. Ultrason. Ferroelectr. Freq. Control **70**, 521 (2023).
21. A. T. Peek, C. Hunter, W. Kreider, T. D. Khokhlova, P. B. Rosnitskiy, P. V. Yuldashev, O. A. Sapozhnikov,

and V. A. Khokhlova, J. Acoust. Soc. Am. **148**, 3569 (2020).

22. T. D. Mast, Acoust. Res. Lett. Open **1**, 37 (2000).
23. C. Pinter, A. Lasso, and G. Fichtinger, Comp. Methods Progr. Biomed. **171**, 19 (2019).
24. F. A. Duck, *Physical Properties of Tissues: A Comprehensive Reference Book* (Academic, New York, 2013).
25. P. A. Hasgall, et al., IT'IS Tissue Properties Database Version 4.1 (2022). https://itis.swiss/virtual-population/tissueproperties/database/acoustic-properties/.
26. J. L. B. Robertson, B. T. Cox, J. Jaros, and B. E. Treeby, J. Acoust. Soc. Am. **141**, 1726 (2017).
27. T. D. Khokhlova and J. H. Hwang, Adv. Exp. Med. Biol. **880**, 83 (2016).
28. P. B. Rosnitskiy, T. D. Khokhlova, G. R. Schade, O. A. Sapozhnikov, and V. A. Khokhlova, IEEE Trans. Ultrason. Ferroelectr. Freq. Control **71**, 341 (2024).
29. B. E. Treeby, J. Jaros, A. P. Rendell, and B. T. Cox, J. Acoust. Soc. Am. **131**, 4324 (2012).
30. O. A. Sapozhnikov, S. A. Tsysar, V. A. Khokhlova, and W. Kreider, J. Acoust. Soc. Am. **138**, 1515 (2015).
31. P. B. Rosnitskiy, P. V. Yuldashev, O. A. Sapozhnikov, L. R. Gavrilov, and V. A. Khokhlova, J. Acoust. Soc. Am. **146** , 1786 (2019).